

Technical Report No. P-84, 1969 (unpublished).

¹⁶J. C. Legg, W. D. Simpson, and S. T. Emerson, Nucl. Phys. **A119**, 209 (1968).

¹⁷P. D. Parker, P. F. Donovan, J. V. Kane, and J. F. Mollenauer, Phys. Rev. Letters **14**, 15 (1965); P. F.

Donovan, Rev. Mod. Phys. **37**, 501 (1965).

¹⁸R. W. Zurmühle, Nucl. Phys. **72**, 225 (1965); R. W. Newsome, Bull. Am. Phys. Soc. **12**, 17 (1967).

¹⁹L. E. Williams, Phys. Rev. **144**, 815 (1966).

R-Matrix Expansion for the Ground-State Energy of a Many-Fermion System*

George A. Baker, Jr., Margaret F. Hind, and Joseph Kahane

Applied Mathematics Department, Brookhaven National Laboratory, Upton, New York 11973

(Received 6 April 1970)

The R -matrix expansion for the ground-state energy of a many-fermion system is carried through fourth order. We evaluate this expansion for a potential modeled after the nucleon-nucleon one. The calculation is described in detail. We find that the "hole-line" approximation seems to underestimate the attraction so that a hard-core force may well be consistent with the experimental binding energy of large nuclei.

1. INTRODUCTION AND SUMMARY

A method, the R -matrix expansion, has recently been proposed^{1,2} for the calculation of the ground-state energy of a many-fermion system interacting through forces which have a short-range strong repulsion, an intermediate-range attraction, and which vanish rapidly at long distances. It is the purpose of this paper to carry through such a calculation for a simple model potential, patterned on the nucleon-nucleon potential. The results of this calculation are compared with those of the two-"hole-line" approximation, and it appears that the "hole-line" approach substantially underestimates the binding energy in this case. Consequently it seems likely that hard-core potentials are compatible with the "observed values" for the binding energy for infinite nuclear matter.

In the second section of this paper we describe how to obtain the R matrix from the potential, both in the absence and presence of an excitation of the Fermi sea. The R matrix is basically the same as Brueckner's³ K matrix except that it has been regularized² in the neighborhood of the Fermi surface to eliminate the appearance of certain singularities which occur in the Brueckner formulation.

Since the R -matrix expansion procedure involves multidimensional integrals of products of the R matrix elements, just as the potential perturbation expansion involved multidimensional integrals of products of the potential matrix elements, we have found it desirable to have an accurate numerical representation of the R matrix. We describe our representation in the third section. As a guide to the proper forms to employ, we compute the di-

lute limiting case, introduce adjustable parameters, and fit them to our values of the matrix elements computed by methods of the second section.

In Ref. 1, the spin and isospin sums were left in matrix form under the integrand of the multidimensional integrals. We have, however, found group-theoretic methods to reduce by mechanical procedures all of these sums (at least through the fourth order in the R expansion) *ab initio*. These procedures are described in the fourth section of this paper.

In the fifth section of our paper we detail how to write out the R -matrix perturbation series and give all the data necessary to construct the multidimensional integrals whose evaluation is required. In the final section we describe our evaluation of these integrals by Monte Carlo methods and tabulate the numerical results. Comparisons are made with the results of other methods.

2. EVALUATION OF THE R MATRIX

In order to evaluate the terms of the R -matrix expansion of the ground-state energy of a many-fermion system which was recently proposed,^{1,2} we need first to evaluate the R matrix itself in terms of an interaction potential. We have selected the following potential for consideration in this paper. First, for states of even relative angular momentum,

$$\begin{aligned} V_T(r) &= V_1, & V_S(r) &= V_2, & 0 < r < c, \\ V_T(r) &= V_3, & V_S(r) &= V_4, & c < r < d, \\ V_T(r) &= V_S(r) &= 0, & & d < r, \end{aligned} \quad (2.1)$$

where V_S is the singlet potential and V_T is the triplet potential. For states of odd relative angular momentum we choose

$$\begin{aligned} V_T(r) &= V_5, \quad V_S(r) = V_6, \quad 0 < r < c, \\ V_T(r) &= V_S(r) = 0, \quad c < r. \end{aligned} \quad (2.2)$$

The parameters in this potential have been chosen as follows:

$$\begin{aligned} c &= 0.4 \text{ F}, \quad d = \frac{29}{7} c, \\ V_1 = V_2 = V_5 = V_6 &= 10^5 \hbar^2 / Mc^2, \\ V_3 &= 1.25 \left(\frac{7}{44} \pi\right)^2 \hbar^2 / Mc^2, \\ V_4 &= 0.96 \left(\frac{7}{44} \pi\right)^2 \hbar^2 / Mc^2. \end{aligned} \quad (2.3)$$

We have fitted the two-body data $a_T = 5.39 \text{ F}$, $r_{0T} = 1.71 \text{ F}$, and $a_S = -23.7 \text{ F}$ to determine these parameters. We compute $E_T = -2.20 \text{ MeV}$, and $r_{0S} = 2.14 \text{ F}$ instead of 2.6 F . Here F is fermi, a is the scattering length, r is the effective range, and E_T is the triplet ground-state energy. The singlet phase shift $\delta_0 = 0$ for k around 150 MeV , instead of 200 MeV as it should. Therefore, our model potential, although too simple to reproduce all of the features of the real two-body nuclear force, is nevertheless sufficiently realistic to lead us to believe that our results are relevant to the understanding of the problem of infinite nuclear matter.

The R -matrix expansion² is basically derived from the Brueckner K -matrix expansion,³ where no self-energy corrections are made to the propagators. Each K matrix in the Brueckner expansion is then expanded in powers of the R matrix, so that every diagram in the K -matrix expansion contributes to every higher-order term in the R -matrix expansion. There are two types of R matrices which enter. The first type involves no excitation of the underlying Fermi sea, and the second type does involve such an excitation. Luckily, through fourth order in R , which is as far as we shall carry the expansion here, in those R 's which involve an excitation of the Fermi sea the excitation is, in an approximation which we will detail below, directly related to the initial or final momentum. We therefore need not introduce an additional parameter to describe the degree of excitation of the Fermi sea. We will denote the R matrix in the presence of this excitation as \hat{R} .

The R matrix² is defined as follows. First we introduce the Green's function

$$\begin{aligned} G_{kl}(r, r') &= \int_0^\infty dk'' \frac{k''^2 j_l(k'' r) j_l(k'' r') - k^2 j_l(kr) j_l(kr')}{k''^2 - k^2} \\ &\quad \times F(p, k'') + k^2 j_l(kr) j_l(kr') / k_F, \end{aligned} \quad (2.4)$$

where k and p are the relative and center of mass momenta of two states in the Fermi sea and $j_l(x)$ is the spherical Bessel function. For a discussion of the definition of R , the reader is referred to Ref. 2. The function $F(p, k'')$ represents the now-standard approximation to the effects of the Pauli exclusion principle and is defined by

$$\begin{aligned} F(p, k'') &= 0, \quad (k''^2 + \frac{1}{4} p^2)^{1/2} < k_F, \\ &= 1, \quad k'' - \frac{1}{2} p > k_F, \\ &= (k''^2 + \frac{1}{4} p^2 - k_F^2) / k'' p, \quad \text{otherwise.} \end{aligned} \quad (2.5)$$

Following Brueckner and Masterson,⁴ we eliminate p completely by using an average value in its place:

$$\frac{1}{4} \bar{p}^2 = \frac{2}{5} k_F^2 (1 - k/k_F) \frac{1 + \frac{1}{2} k/k_F + \frac{1}{6} k^2/k_F^2}{1 + \frac{1}{2} k/k_F}, \quad (2.6)$$

where again $k \leq k_F$. From the Green's function and the interaction potential, we define a wave function

$$u_{kl}(r) = j_l(kr) - \frac{2}{\pi} \int_0^\infty G(r, r') V(r') u_{kl}(r') r'^2 dr'. \quad (2.7)$$

We remark that V depends on l by (2.1) and (2.2), and also that there will, of course, be separate singlet and triplet wave functions determined by using the singlet and triplet potentials in (2.7). From the wave functions we obtain the R matrix elements, as

$$\langle k' | R_l | k \rangle = \frac{2}{\pi} \int_0^\infty j_l(k' r) V(r) u_{kl}(r) r^2 dr, \quad (2.8)$$

where $k \leq k_F$, and k' is unrestricted. If we define

$$l(k) = \int_0^\infty \frac{k^2 dk''}{k''^2 - k^2} F(\bar{p}, k'') - \frac{k^2}{k_F} \quad (2.9)$$

then² the K matrix elements can be given as

$$\langle k' | K_l | k \rangle = \langle k' | R_l | k \rangle / [1 + l(k) \langle k | R_l | k \rangle] \quad (2.10)$$

in terms of those for R . Equation (2.10) readily gives us the expansion

$$\begin{aligned} \langle k' | K_l | k \rangle &= \langle k' | R_l | k \rangle \{ 1 - l(k) \langle k | R_l | k \rangle \\ &\quad + [l(k) \langle k | R_l | k \rangle]^2 - \dots \} \end{aligned} \quad (2.11)$$

of the K matrix in powers of the R matrix.

The contribution to the single-particle energies made by the K matrix, i.e., the sum of the ladder diagrams, is given by

$$\begin{aligned} E(m) = & \frac{1}{2}m^2 + 4 \left[\int_0^{\frac{1}{2}(k_F - m)} 2Ik^2 dk \right. \\ & \left. + \int_{\frac{1}{2}(k_F - m)}^{\frac{1}{2}(k_F + m)} \left(1 - \frac{m^2 + 4k^2 - k_F^2}{4km} \right) Ik^2 dk \right], \end{aligned} \quad (2.12)$$

where

$$\begin{aligned} I = & \frac{1}{2} \left[\sum (2l+1) \begin{pmatrix} 3 & l \text{ even} \\ 1 & l \text{ odd} \end{pmatrix} \langle k | K_{S, l} | k \rangle \right. \\ & \left. + \sum (2l+1) \begin{pmatrix} 3 & l \text{ even} \\ 9 & l \text{ odd} \end{pmatrix} \langle k | K_{T, l} | k \rangle \right] \end{aligned} \quad (2.13)$$

with S and T standing for the singlet and triplet states. By K in (2.13) we mean the series expansion (2.11) in powers of the R matrix. This series is divergent, though summable^{5,6} for suitable potential interactions. The divergence arises² from the divergence of $l(k)$ as k tends to k_F . The integral (2.12) nonetheless converges in every finite order in R . It is to be remembered that the K -matrix expansion in powers of V is divergent,⁵ and the R -matrix expansion² in powers of V is convergent, so that the divergence of $K(R)$ is expected. This type of rearrangement of an infinite, divergent series has been discussed in another place⁶ and found legitimate. The contribution to the ground-state energy made by the ladder diagrams via the R -matrix expansion of (2.12) is given by

$$E_0 = \frac{3}{2k_F^3} \int_0^{k_F} [E(m) - \frac{1}{2}m^2] m^2 dm. \quad (2.14)$$

Through fourth order in K we may use the following special feature to restrict the number of parameters on which the R matrix in the presence of an excited Fermi sea depends. To this order, every excitation consists of a single filled-state hole pair which combines with one filled state at the previous or next vertex to form an unexcited Fermi sea. Therefore, except for a hole momentum, which we must integrate over in any case, the excitation energy is directly related by momentum conservation to either the initial or final relative momentum at that vertex. Hence, by averaging over the allowed values of the hole momentum in a manner similar to (2.6), we may again reduce the R matrix to a dependence only on k , k' , and l . If one wishes to proceed to higher order than four, one must then know R as a general function of the excitation energy. One further special simplification is available on this account. One finds (we

will see this result below) that the averaged excitation energy always exceeds the energy of the incident state, so that R and K are equal in this case. The calculational formulas are now²

$$\hat{G}_{k, l}(r, r') = \int_0^\infty k''^2 dk'' \frac{j_l(k''r) j_l(k''r')}{k''^2 + \Delta(k)} \hat{F}(p, k''), \quad (2.15)$$

where \hat{F} , by approximating the Pauli principle in the same manner as F , has been extended to values of p outside the Fermi sea to be

$$\begin{aligned} \hat{F}(p, k'') = & 1, \quad \frac{1}{2}p - k_F > k'', \\ = & 0, \quad (k''^2 + \frac{1}{4}p^2)^{1/2} < k_F, \\ = & 1, \quad k'' - \frac{1}{2}p \geq k_F, \\ = & (k''^2 + \frac{1}{4}p^2 - k_F^2)/k''p, \quad \text{otherwise.} \end{aligned} \quad (2.16)$$

The definition of the average value of p changes, because we now have a vertex with one incident filled-state line instead of an unexcited Fermi sea as in (2.6). It is

$$\begin{aligned} \frac{1}{4}\bar{p}^2 = & (k_F^4 + k^4/15^2)/(k_F^2 - \frac{1}{3}k^2), \quad k < k_F, \\ = & k^2 + \frac{3}{5}k_F^2, \quad k \geq k_F. \end{aligned} \quad (2.17)$$

As $\bar{p} > k_F$ always, it follows from (2.16) that F is never zero. The value of $\Delta(k)$ is, basically, $(2k)^2 - (k)^2 +$ mean-square average of a hole momentum. The average is restricted by the given value of k . This quantity works out to be

$$\begin{aligned} \Delta(k) = & 3k^2 + \frac{k_F^4 - \frac{4}{3}k_F^3k + k_F^2k^2 - \frac{4}{15}k^4}{k_F^2 - \frac{1}{3}k^2}, \quad k < k_F, \\ = & 3k^2 + \frac{3}{5}k_F^2, \quad k \geq k_F. \end{aligned} \quad (2.18)$$

The wave function and R matrix follow in the same manner as above:

$$\hat{u}_{k, l}(r) = j_l(kr) - \frac{2}{\pi} \int_0^\infty \hat{G}_{k, l}(r, r') V(r') \hat{u}_{k, l}(r') r'^2 dr', \quad (2.19)$$

$$\langle k' | \hat{R}_l | k \rangle = \frac{2}{\pi} \int_0^\infty j_l(k'r) V(r) \hat{u}_{k, l}(r) r^2 dr. \quad (2.20)$$

Through the use of these formulas, we can produce any desired matrix element numerically by use of a high-speed digital computer. (We have used the Brookhaven CDC 6600.) The numerical procedures used are the following. In the calculation of the Green's function for R [Eq. (2.4)] we used a step size of $\Delta k'' = 0.1k_F$ and did a Simpson's rule integration to $k'' = 10k_F$. For the contribution to G from the remainder of the range, an asymp-

otic formula previously derived⁷ was used, plus the analytic integral of the part not represented thereby. For \hat{G} we break up Eq. (2.15) as

$$\begin{aligned} \hat{G}_{kl}(r, r') = & \int_0^\infty k''^2 dk'' \frac{j_l(k''r) j_l(k''r')}{k''^2 + \Delta(k)} \\ & + \int_0^{k_F + \frac{1}{2}\bar{p}} k''^2 dk'' \frac{j_l(k''r) j_l(k''r')}{k''^2 + \Delta(k)} \\ & \times [\hat{F}(p, k'') - 1], \end{aligned} \quad (2.21)$$

since by (2.16) $\hat{F} = 1$ for $k'' > k_F + \frac{1}{2}\bar{p}$. The first term in (2.21) can be evaluated analytically, and it yields

$$\int_0^\infty k''^2 dk'' \frac{j_l(k''r) j_l(k''r')}{k''^2 + \Delta(k)} = \lambda i_l(\lambda r_<) k_l(\lambda r_>), \quad (2.22)$$

where $\lambda^2 = \Delta(k)$ and where i_l and k_l are spherical Bessel functions of imaginary argument of the first and third kinds. That is,

$$i_l(x) = \sqrt{\frac{1}{2}\pi/x} I_{n+1/2}(x), \quad i_0(x) = (\sinh x)/x, \quad (2.23)$$

$$k_l(x) = \sqrt{\frac{1}{2}\pi/x} K_{n+1/2}(x), \quad k_0(x) = (\frac{1}{2}\pi/x)e^{-x}.$$

Again we have used a step size of $\Delta k'' = 0.1k_F$ and a Simpson's-rule integration. To solve the integral equations (2.7) and (2.19), a mesh size of $\Delta r = \Delta r' = \frac{1}{7}c$ was used. For our potential this choice requires, for each value of k and l , the inversion of a 29×29 matrix for l even and a 7×7 matrix for l odd. The wave functions were computed for $0 \leq k \leq k_F$ at steps of $\frac{1}{20}k_F$, and from them the necessary values of $\langle k' | R | k \rangle$ were computed by a Simpson's-rule integration of (2.8) and (2.20). The range of k was extended for \hat{R} well beyond k_F , though in coarser steps.

3. REPRESENTATION OF THE R MATRIX

In the previous section we have described how to evaluate the necessary R matrix elements. As we plan to evaluate many multidimensional integrals in which R matrix elements appear in the integrand, it is important to have an empirical representation of these elements so that the numerical aspects of this problem can be reduced to manageable proportions.

We shall first treat the problem of representing the R matrix with no excitation in the Fermi sea. As a guide to what behavior is to be expected, we will compute the limiting behavior for a dilute system ($k_F \rightarrow 0$). We expect, physically, that this approximation will also be valid when $0 < k_F \ll k$, as

the scattering should not be much affected when the energy is large compared to that in the Fermi sea. For a simple hard-core potential, one can easily derive (θ is the angle between \vec{k} and \vec{k}')

$$\langle \vec{k}' | R | \vec{k} \rangle = -\frac{1}{k} \sum_{l=0}^{\infty} (2l+1) P_l(\cos\theta) j_l(k'c) / n_l(kc). \quad (3.1)$$

The standing-wave normalization² has been used,

$$u_l(r) = kr [j_l(kr) - \tan\delta_l n_l(kr)], \quad r \rightarrow \infty, \quad (3.2)$$

together with the Schrödinger equation

$$\frac{d^2 u_l(r)}{dr^2} + \left[k^2 - U(r) - \frac{l(l+1)}{r^2} \right] u_l(r) = 0, \quad (3.3)$$

$$U(r) = (m/\hbar^2)V(r), \quad mE = \hbar^2 k^2$$

for $u_l(r)$, the l th partial wave, and the formula⁸

$$\langle \vec{k}' | R | \vec{k} \rangle = \frac{1}{2\pi^2} \int d^3r e^{-i\vec{k}' \cdot \vec{r}} V(r) \psi_{\vec{k}}(\vec{r}), \quad (3.4)$$

where ($\hat{\theta}$ is the angle between \vec{r} and \vec{k})

$$\psi_{\vec{k}}(\vec{r}) = \frac{1}{kr} \sum_{l=0}^{\infty} (2l+1) i^l u_l(r) P_l(\cos\hat{\theta}). \quad (3.5)$$

Examining (3.1) closely and remembering that $k \leq k_F$ for the problems of interest, we see that the series (3.1) converges rapidly for any value of k' . This result suggests that a partial-wave expansion of $\langle \vec{k}' | R | \vec{k} \rangle$ of a finite number of terms will be sufficient to represent R . We expect, as mentioned above, that the $k_F = 0$ approximation will be good at large k' . One can also work out the $k_F = 0$ approximation where there is an attractive potential outside a hard core, as in (2.1). We will let

$$W = V_3 \text{ or } V_4, \quad \beta^2 = \frac{MW}{\hbar^2} + k^2, \quad (3.6)$$

respectively, for triplet or singlet states. It is to be noted that β may be imaginary, since W is negative. Then

$$\begin{aligned} \frac{M \langle k' | R | k \rangle}{\hbar^2} = & \frac{\Re}{\beta^2 - k'^2} [f_1 j_1(k'd) - f_2 k' j_{l-1}(k'd) \\ & + (k^2 - k'^2) j_l(k'c)], \end{aligned} \quad (3.7)$$

where

$$f_1 = (\beta d)^2 [j_1(\beta c) n_{l-1}(\beta d) - n_l(\beta c) j_{l-1}(\beta d)] (\beta^2 - k^2), \quad (3.8)$$

$$f_2 = \beta d^2 [j_1(\beta c) n_l(\beta d) - n_l(\beta c) j_1(\beta d)] (\beta^2 - k^2).$$

The distance d is the range of the potential (2.1). In the $k_F=0$ approximation, \mathcal{R} is determined by matching the solution to the form (3.2) at $r=d$. In order to get a good representation of the values of $\langle k'|R_l|k\rangle$, we have adopted the following procedure. For l even, we have fitted our R -matrix data with the form (3.7), allowing β and the wave-function normalization as adjustable parameters, and determined them as a function of k for $k=0, 0.1k_F, \dots, k_F$. We fitted over the range $0 \leq k' \leq 5k_F$ and then compared our extrapolations out to $10k_F$. We did not, however, fit $l=0$, $0 \leq k \leq k_F$, $0 \leq k' \leq k_F$, but rather have used a table of values and bilinear interpolation in this range. Over-all, the quality of the fit obtained varied between $\frac{1}{2}$ and 2%, measured in units of the local maximum. The β 's showed weak but non-negligible variation with k_F , k , and l . The same general form was used for odd values of l , except that here $f_1=f_2=0$, and $\beta^2=k^2$, since according to (2.2) there is only a hard core and no attraction. Consequently there is only one adjustable parameter, \mathcal{R} . Here the fit is good to about 3%. We have found for the range of densities considered that truncating the expansion

$$\langle \vec{k}'|R|\vec{k}\rangle = \sum_{i=0}^{\infty} (2l+1)P_l(\cos\theta)\langle k'|R_l|k\rangle \quad (3.9)$$

at $l=3$ provides adequate accuracy, comparable to that of the individual partial waves.

We will now consider the problem of adequately representing the \hat{R} matrix, when an excitation of the Fermi sea is present. Here a fit is required throughout the (k, k') plane. Again, it is instructive to compute the $k_F=0$ approximation as a guide to the structure of the \hat{R} matrix. This approximation can be obtained as the solution of (2.21) of Ref. 1, namely,

$$(-\nabla^2 + q^2)\psi_{\vec{k}}^*(\vec{r}) + U(r)\psi_{\vec{k}}(\vec{r}) = (k^2 + q^2)e^{i\vec{k}\cdot\vec{r}}, \quad (3.10)$$

where U is as in (3.3) and q^2 is the excitation energy. The expansion of this equation in partial waves, its solution, and finally taking the hard-core limit are tedious but elementary operations, and we shall omit the details. The excitation energy (2.18) is

$$q^2 = \Delta(k) + k^2. \quad (3.11)$$

We find it convenient to define the quantities

$$\begin{aligned} \kappa^2 &= \Delta(k) - mW/\hbar^2, \\ \lambda^2 &= \Delta(k), \end{aligned} \quad (3.12)$$

where W is as in (3.6). (Note that W is negative.) Working out the details we obtain

$$\begin{aligned} \frac{M\langle k'|\hat{R}_l|k\rangle}{\hbar^2} &= \frac{2}{\pi} \frac{k'^2 + \lambda^2}{k'^2 + \kappa^2} [c^2(k^2 + \lambda^2)V_1 + c^2Q_l j_l(k'c) \\ &\quad + d^2V_2 + (\kappa^2 - \lambda^2)(k^2 + \kappa^2)d^2T_l V_3], \end{aligned} \quad (3.13)$$

where

$$\begin{aligned} V_1 &= \frac{k j_l(k'c) j_{l-1}(kc) - k' j_{l-1}(k'c) j_l(kc)}{k'^2 - k^2}, \quad k \neq k', \\ &= \frac{1}{2} c [j_l^2(kc) - j_{l+1}(kc) j_{l-1}(kc)], \quad k = k', \\ V_2 &= \frac{k j_l(k'd) j_{l-1}(kd) - k' j_{l-1}(k'd) j_l(kd)}{k'^2 - k^2}, \quad k \neq k', \\ &= \frac{1}{2} d [j_l^2(kd) - j_{l+1}(kd) j_{l-1}(kd)], \quad k = k', \\ V_3 &= \frac{2 \lambda j_l(k'd) k_{l-1}(\lambda d) + k' j_{l-1}(k'd) k_l(\lambda d)}{\pi (k'^2 + \lambda^2)}. \end{aligned} \quad (3.14)$$

The symbols Q_l and T_l are parameters determined by matching boundary conditions and are hence independent of k' . We have divided the region into two parts for the purpose of a fit: the small- k range, $0 \leq kc \leq 3$, $0 \leq k'c \leq 5$; and the large- k range, which is the rest of the positive quadrant in the (k, k') plane.

In the small- k range we have fitted on a mesh $\Delta k = \Delta k' = 0.1/c$ with the form

$$\langle k'|\hat{R}_l|k\rangle = \sum_{i=1}^4 \mathcal{R}_i A_i(k'), \quad (3.15)$$

where the \mathcal{R}_i are adjustable parameters and

$$\begin{aligned} A_1(k') &= \frac{2}{\pi} \frac{k'^2 + \lambda^2}{k'^2 + \kappa^2} c^2 j_l(k'c), \\ A_2(k') &= \frac{2}{\pi} \frac{(k'^2 + \lambda^2)(k^2 + \lambda^2)}{k'^2 + \kappa^2} c^2 V_1, \\ A_3(k') &= \frac{2}{\pi} \frac{k'^2 + \lambda^2}{k'^2 + \kappa^2} d^2 V_2, \\ A_4(k') &= \frac{2}{\pi} \frac{(\kappa^2 - \lambda^2)(k'^2 + \lambda^2)(k^2 + \kappa^2)}{k'^2 + \kappa^2} d^2 V_3. \end{aligned} \quad (3.16)$$

We have adjusted the \mathcal{R}_i by least squares over the range $0 \leq k' \leq 5/c$ on a mesh of $0.1/c$; the range of k is $0 \leq k \leq 3/c$ on a mesh of $0.1/c$. We obtained a fit accurate to about 3% over this range.

This expression can be recast to display its explicit dependence on k' . Linear interpolation in k can then be used to obtain the values in the small- k range.

$$\begin{aligned} \frac{M\langle k'|\hat{R}|k\rangle}{\hbar^2} &= \frac{k'^2 + \lambda^2}{k'^2 + \kappa^2} [r_1 j_l(k'c) + \alpha(k')] \\ &\quad + \frac{1}{k'^2 + \kappa^2} [r_6 j_l(k'd) + r_7 k' j_{l-1}(k'd)], \end{aligned} \quad (3.17)$$

where

$$\begin{aligned} \alpha(k') &= \frac{1}{k'^2 - k^2} [r_2 j_l(k'c) + r_3 k' j_{l-1}(k'c) \\ &\quad + r_4 j_l(k'd) + r_5 k' j_{l-1}(k'd)], \quad k' \neq k, \\ &= -\frac{1}{2} c [r_3 j_l(k'c) + r_2 j_{l+1}(k'c)/k'] \\ &\quad - \frac{1}{2} d [r_5 j_l(k'd) + r_4 j_{l+1}(k'd)/k'], \quad k' = k \end{aligned} \quad (3.18)$$

and the r_j are functions of k alone and not of k' . The relation between the r_i and the \mathcal{R}_i is easily obtained from (3.14)–(3.18).

For the odd- l states, where only a hard core is present, the problem is much simpler. Taking the hard-core limit in Sec. 3 of Ref. 1, we deduce in the $k_F = 0$ approximation

$$\begin{aligned} \frac{M\langle k'|\hat{R}_l|k\rangle}{\hbar^2} &= \frac{2}{\pi} c^2 (k^2 + \gamma^2) V_1 \\ &\quad + \frac{2}{\pi} [kc j_{l-1}(kc) - H_l j_l(kc)] j_l(k'c), \end{aligned} \quad (3.19)$$

$$H_l = -\lambda k_{l-1}(\lambda c)/k_l(\lambda c).$$

We have fitted the \hat{R} matrix using a least-squares fit for two parameters. These parameters were inserted in (3.19) where the factors of $(2/\pi)$ appear. We obtained results accurate usually to a few hundredths of a percent ranging up to 0.2%. We can recast (3.19) in a form to make the dependence on k' manifest. It is

$$\frac{M\langle k'|\hat{R}|k\rangle}{\hbar^2} = c_1 j_l(k'c) + B(k'), \quad (3.20)$$

where

$$\begin{aligned} B(k') &= \frac{1}{k'^2 - k^2} [c_2 j_l(k'c) + c_3 k' j_{l-1}(k'c)], \quad k' \neq k, \\ &= -\frac{1}{2} c [c_3 j_l(k'c) + c_2 j_{l+1}(k'c)/k'], \quad k' = k, \end{aligned} \quad (3.21)$$

and again the c 's are independent of k' . Over the small- k range we found it sufficient to keep $l \leq 14$ for l even, and $l \leq 5$ for l odd.

For the large- k range we have developed an as-

ymptotic formula to represent the \hat{R} matrix. One would expect that at the higher energies involved that the matrix elements would be dominated by the effects of the hard core. To investigate this we compared, in the range $3k_F \leq k \leq 5k_F$, the differences between the \hat{R} matrix for hard core alone and for hard core plus attraction. We found, for the partial waves checked, agreement within about 3%. Besides, in this range, the contribution to the final integrals to be done will be small, because of the presence of other factors which go to zero.

In order to develop an asymptotic formula, we propose to sum the $k_F = 0$ approximation (3.19) to all orders in l . First we will insert an approximation for H_l . One can easily show from (2.23), (3.19), and

$$k_1(x) = (\pi/2x)e^{-x}[1 + (1/x)] \quad (3.22)$$

that

$$H_0 \approx -\lambda c \quad (3.23)$$

for large λ , or equivalently $k \gg 1$. If we use the standard recursion relations for Bessel functions,⁸ one can show that

$$H_{l+1} = -\lambda^2 c^2 / (2l + 1 - H_l) \quad (3.24)$$

exactly. If we make the hypothesis that

$$H_l = -\lambda c + l, \quad (3.25)$$

then expanding (3.24) for λ large confirms (3.25) for $l+1$ within $O(\lambda^{-1})$. In this approximation, we will show that (3.19) sums to

$$\begin{aligned} \frac{M\langle \vec{k}'|\hat{R}|\vec{k}\rangle}{\hbar^2} &= \frac{2c}{\pi} \left[(\lambda^2 + \vec{k} \cdot \vec{k}') c^2 \frac{j_1(|\vec{k} - \vec{k}'|c)}{|\vec{k} - \vec{k}'|c} \right. \\ &\quad \left. + (\lambda c + 1) j_0(|\vec{k} - \vec{k}'|c) \right]. \end{aligned} \quad (3.26)$$

Now to show that (3.26) is equivalent to (3.19) using (3.25), we first note that⁸

$$\frac{j_1(x)}{x} = \int_0^1 j_0(x\xi) \xi^2 d\xi, \quad (3.27)$$

which, together with the partial-wave expansion

$$j_0(|\vec{k} - \vec{k}'|c) = \sum_{n=0}^{\infty} (2l+1) P_l(\cos \theta) j_l(kc) j_l(k'c) \quad (3.28)$$

and the observation that

$$k \frac{\partial}{\partial k} [j_0(|\vec{k} - \vec{k}'|c)] = (k^2 - \vec{k} \cdot \vec{k}') \frac{j_1(|\vec{k} - \vec{k}'|c)}{|\vec{k} - \vec{k}'|c}, \quad (3.29)$$

allows us, by interchanging the order of summation and integration on differentiation, to write (3.26) as

$$\begin{aligned} \frac{M(\vec{k}'|\hat{R}|\vec{k})}{\hbar^2} &= \frac{2c}{\pi} \sum_{l=0}^{\infty} (2l+1) P_l(\cos\theta) [k c j_{l-1}(k c) j_l(k' c) \\ &+ (\lambda^2 c^2 + k^2 c^2) \int_0^1 j_l(k c x) j_l(k' c x) x^2 dx \\ &+ (\lambda c - l) j_l(k c) j_l(k' c)], \end{aligned} \quad (3.30)$$

where the recursion relation⁸

$$j_l'(x) = j_{l-1}(x) - \frac{l+1}{x} j_l(x) \quad (3.31)$$

has been used. When we recognize the integral in (3.30) as having⁹ the value (V_1/c) , then we see that (3.30) is equivalent to (3.19), where (3.25) is used for H_l . Thus the approximations in using (3.26) as an asymptotic form are these: (i) $k_F \approx 0$, (ii) H_l is given by (3.25), and (iii) that the hard core gives the dominant scattering effect. We have also compared (3.26) [as expanded (3.30)] with our numerical results, and for the l values we have checked we find an accuracy of about 3% or better over the range $3/c \leq k \leq 5/c$. We have therefore adopted this asymptotic form for the large- k range.

4. GROUP-THEORETIC REDUCTION OF THE SUMS OVER SPIN AND ISOSPIN SPACE

In the evaluation of the contributions to the R -matrix expansions, in addition to the integrals over the intermediate momenta, one must sum over the various spin and isospin states. Through fourth order in R , up to four independent spins and isospins can occur, or 256 different states. Although this sum needs to be performed only once for each diagram, the formulas that result are rather awkward and may indeed contain as many as 256 terms. We will show how these formulas may be derived in a simple and compact fashion (at least through fourth order).

We first need to give a formalism which correctly takes account of the contributions from the different states. It will be helpful to have an example to illustrate the discussion. We choose the diagram III.8.⁷ The Hugenholtz diagram is shown in Fig. 1. This diagram represents the sum of a number of basic diagrams, each of which is an exchange variation of the Hugenholtz diagram. These are obtained by expanding each vertex into the form shown in Fig. 2. The X's at the top and bot-

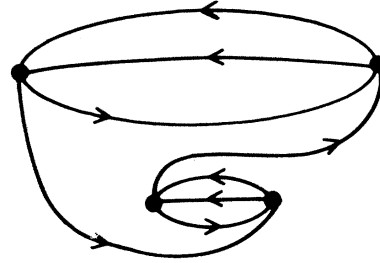


FIG. 1. The Hugenholtz diagram representing case III.8.

tom represent two states each. Each of the four states involved changes its occupation during the interaction. If a state in the Fermi sea is emptied, its line enters on the left as a blank and leaves on the right as dotted. If, on the other hand, it is filled, it enters on the left as a dotted line and leaves on the right as a blank. For a state above the Fermi sea, if it is filled it enters blank and leaves as a solid line; conversely, if it is emptied, it enters as a solid line and leaves as a blank line. Thus one representative of III.8 becomes as illustrated in Fig. 3.

For clarity, we will first explain the action of the vertices (labeled V_1-V_4) for the spin- and isospin-independent case. Before any vertex acts, the system is represented by a Slater determinant with one row for each occupied momentum state. The action of the first vertex multiplies the wave function by a factor and replaces the momentum variables labeled \vec{m} and \vec{n} in the determinant by new ones labeled \vec{v} and $\vec{\mu}$, respectively. Of course, we must integrate over appropriate ranges of \vec{m} , \vec{n} , \vec{v} , and $\vec{\mu}$, but we will treat this aspect in a later section. The action of the successive vertices is outlined in Table I. We have numbered the rows in the Slater determinant 1-4 and the originally empty states which are later filled 5-8. These types are separated by a dashed vertical line. As every allowed vertex in a Hugenholtz diagram is four pronged, there will always be exactly $2n$ columns in such a table where n is the number of vertices, although there need not be equal numbers of the two types. The symbols P_{ij} standing in the right-most column are permutation operators on the $2n$ position numbers. One sees that the effect



FIG. 2. Expanded vertex.

of a vertex can be thought of in terms of these permutation operators. Any valid perturbation term must result in a final wave function which is not orthogonal to the original one; by the orthogonality properties of Slater determinants the first four entries on the last line of Table I must therefore be the same, though possibly in different order, as those in first line. In other words, the permutation

$$(P_{15} P_{26})(P_{37} P_{48})(P_{37} P_{46})(P_{15} P_{28}) = (P_{11})(P_{33})(P_{24})(P_{55})(P_{77})(P_{68}) \quad (4.1)$$

representing the action of all the vertices must factor into a permutation of 1-4 times a permutation of 5-8, as indeed we see in (4.1) that it does for our example. When there are spin variables attached to the momentum variables, we get $(2S+1)^C$ such allowed states, where C is the number of cycles in the permutation of (1-4). In our example $C=3$. This count arises from noting that there is one independent spin per cycle, and there are $(2S+1)$ allowed states per spin. In our problem we will deal with $S=\frac{1}{2}$, of course. A similar result is also obtained for the inclusion of isospin with a factor of $(2I+1)^C$ for those states. Now, as every Hugenholtz diagram corresponds to many exchange terms, we wish to write out the sum of all such terms represented by one diagram in one simple form. This task may be done as

$$2^{n-m} \prod_{j=n}^1 [(R_{D,j}I + R_{E,j}P_{m_j, n_j}P_{\mu_j \nu_j})P_{m_j \nu_j}P_{n_j \mu_j}] |s\rangle, \quad (4.2)$$

where $|s\rangle$ is the Slater determinant, $R_{D,j}$ and $R_{E,j}$ are the coefficients for the direct and exchanged vertex configurations, n is the number of vertices, and m the number of pairs of equivalent lines. The lines are labeled conventionally as in Fig. 3 where, for example, $m_3 \equiv \nu_2$, $\nu_4 \equiv m_1$, etc. There will be $2n$ such relations, as each end of $2n$ lines is given

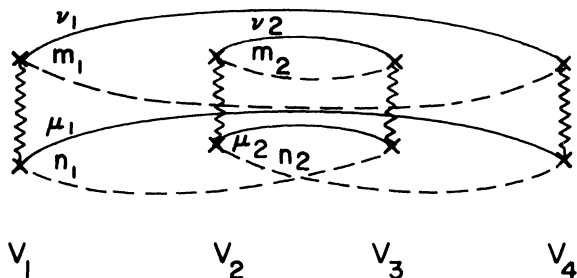


FIG. 3. One representative of the class of expanded diagrams represented by Fig. 1. The line labels give the momenta and the V_i label the vertices in order.

a separate name in the above (4.2) labeling scheme. It is these relations, of course, which distinguish an individual graph.

Let us now consider the addition of a spin-dependent force. We wish to consider only those forces which conserve the total spin at a vertex. When $S=\frac{1}{2}$, spin exchange is the only possible such force. It is convenient to write

$$P_{ij} = P_{ij}(\kappa)P_{ij}(\sigma)P_{ij}(\iota), \quad (4.3)$$

where κ, σ , and ι stand for momentum, spin, and isospin, respectively, and the permutation operator now permutes only the quantity specified by the argument. When we recognize that there is a factor of $(-1)^q$, where q is the number of permutations required to express (4.2) as a coordinate independent multiple of $|s\rangle$, we can replace $P_{ij}(\kappa)$ by (-1) inside the parentheses in (4.2) provided we remember to take account of the over-all sign of the basic diagram representative of the Hugenholtz diagram we have chosen. Consequently, the contribution of a single vertex will be, in terms of the singlet and triplet terms

$$\begin{aligned} & [\frac{1}{2}(R_T + R_S)_{D,j}I + \frac{1}{2}(R_T - R_S)_{D,j}P_{m_j n_j}(\sigma)P_{\mu_j \nu_j}(\sigma) \\ & - \frac{1}{2}(R_T + R_S)_{E,j}P_{m_j n_j}(\sigma)P_{m_j n_j}(\iota)P_{\mu_j \nu_j}(\sigma)P_{\mu_j \nu_j}(\iota) \\ & - \frac{1}{2}(R_T - R_S)_{E,j}P_{m_j n_j}(\iota)P_{\mu_j \nu_j}(\iota)]. \quad (4.4) \end{aligned}$$

The contribution for a given Hugenholtz diagram is then given as follows. Multiply the factors (4.4) together (in proper order) for all the vertices in the Hugenholtz diagram. The result will be a sum of terms each of which is a coefficient times an element of the direct product of the permutation group on spins and that on isospins on the $2n$ line names. Each element can be factored into the product of permutations on initially filled states only, and of permutations on initially empty states only. Now

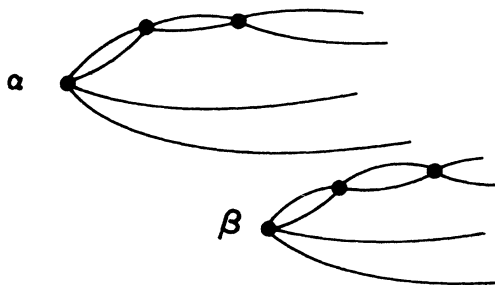


FIG. 4. Subdiagrams which occur in all possible relative vertex orders when the sum over all allowed diagrams is taken.

TABLE I. Vertex action in III. 8.

	1	2	3	4	5	6	7	8	
V_1	m_1	n_1	m_2	n_2	ν_1	μ_1	ν_2	μ_2	$P_{15} P_{26}$
V_2	ν_1	μ_1	m_2	n_2	m_1	n_1	ν_2	μ_2	$P_{37} P_{48}$
V_3	ν_1	μ_1	ν_2	μ_2	m_1	n_1	m_2	n_2	$P_{37} P_{46}$
V_4	ν_1	μ_1	m_2	n_1	m_1	μ_2	ν_2	n_2	$P_{15} P_{28}$
	m_1	n_2	m_2	n_1	ν_1	μ_2	ν_2	μ_1	

take the trace of the matrix representation of the permutation operators induced in the space of spin and isospin states corresponding to the originally filled states. (Note that permutations of one empty state into another are unity in this representation.)

We digress from our reductions at this point to remark that it follows at once that the Hugenholtz theorem,⁹ which states that if a perturbation term has two portions α and β as in Fig. 4, then when one sums over all the possible vertex orders the result is just the product of the two parts taken separately. The different possible vertex orders arise because all those different diagrams are possible which retain the order of the α vertices and the β vertices but allow any relative order between the α and β vertices. This theorem is important, as it eliminates the extra complication of an excited Fermi sea in the calculation of the contributions of both the α and β vertices. This theorem goes through because the permutation operators at the α and β vertices are on disjoint sets and so commute.

We can, at least through fourth order, make the following reduction. We would like to reduce the basis for the permutation operators as far as possible. Inasmuch as the trace of the permutation operators is always 2^C , where C is the number of cycles in the final permutation, we cannot expect to reduce the basis below 2^M , where M is the maximum number of cycles. We propose the following scheme.

Suppose that the Hugenholtz diagram is such that we can draw a basic diagram which has the maximum number of cycles (closed loops made of solid or dashed lines only) with the additional property

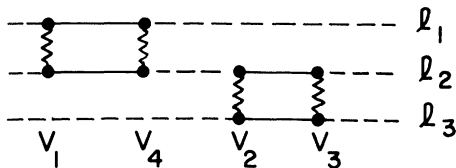


FIG. 5. Reduced form of an expanded representative of a straightenable diagram.

that a vertex order can be specified so that every cycle (loop) is traversed in order. (For Fig. 3 such an order is V_1, V_4, V_2, V_3 .) We call these *straightenable graphs*. By inspection, all fourth-order graphs are of this type, but not all fifth-order ones. We illustrate by straightening out Fig. 3 (which is a suitable maximum-loop basic diagram for Fig. 1) in Fig. 5. The loop lines as shown may be either solid or dashed. The left and right sides are supposed to be connected on the same level. Now, if there is an interchange at V_1 and V_2 only, the lines are crossed at those points, and a single loop results. If an interchange at V_1 and V_4 only occurs, the two crossed lines undo each other and there are again three separate loops. If we consider any straightforward graph which can be drawn in the form of Fig. 5 (horizontal loop lines with pair interactions between them, in order), then if we replace a vertex with

$$\begin{aligned} & \left[\frac{1}{2}(R_T + R_S)_{D,j} I + \frac{1}{2}(R_T - R_S)_{D,j} P_{I_j, \lambda_j}(\sigma) \right. \\ & \quad - \frac{1}{2}(R_T + R_S)_{E,j} P_{I_j, \lambda_j}(\sigma) P_{I_j, \lambda_j}(\tau) \\ & \quad \left. - \frac{1}{2}(R_T - R_S)_{E,j} P_{I_j, \lambda_j}(\tau) \right], \end{aligned} \quad (4.5)$$

where I_j, λ_j are the interacting loop numbers at vertex j (taken in straightened order), we will obtain the correct statistical weight by taking the trace in the space of states where each loop is assigned one independent spin and isospin.

We are now in a position to express the contribution of a Hugenholtz diagram in a way which can be greatly simplified by group theory. Let

$$\begin{aligned} R_{j1} &= \frac{1}{2}(R_T + R_S)_{D,j}, \\ R_{j2} &= \frac{1}{2}(R_T - R_S)_{D,j}, \\ R_{j3} &= \frac{1}{2}(R_T + R_S)_{E,j}, \\ R_{j4} &= \frac{1}{2}(R_T - R_S)_{E,j}. \end{aligned} \quad (4.6)$$

Then the contribution is

$$\text{Tr} \left[\prod_{k=1}^n (R_{k1} I \times I + R_{k2} I \times M_k - R_{k3} M_k \times M_k - R_{k4} M_k \times I) \right], \quad (4.7)$$

where $M_k = U(P_{I_k, \lambda_k})$, the representative in loop-spin space. The second term in the direct product is for isospin space, but the representation here is identical to that in spin space. Now (4.7) is a polynomial of degree n in the R_{kj} . It has the 4^n terms in which one of the four values of j appears with each value of $k=1, \dots, n$ in the subscripts in

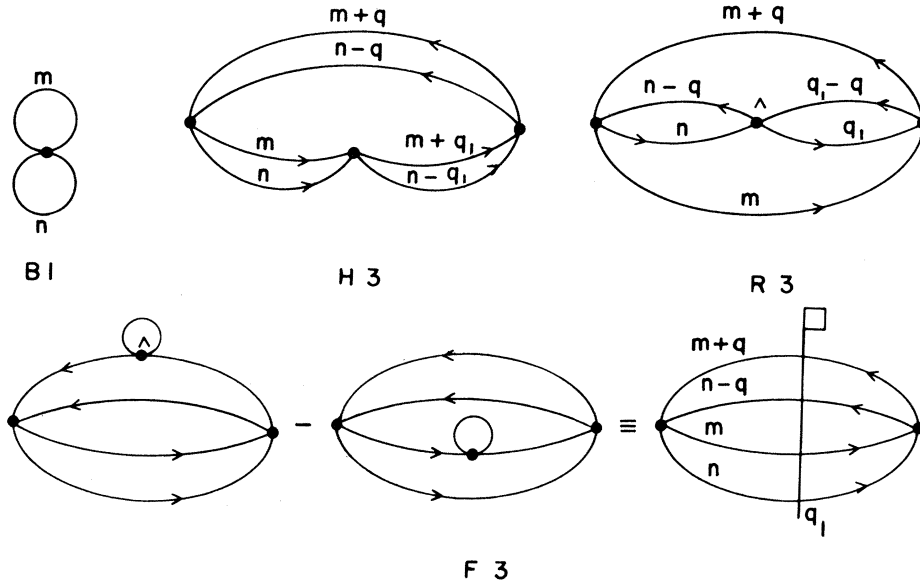


FIG. 6. R -matrix diagrams for the first three orders in the expansion.

the product. Our task is to produce these coefficients. We note that they can be obtained in turn by setting, for each k , one of the $R_{kj} = 1$ and taking the rest of the R 's to be zero. In this circumstance, there is only one term in (4.7), and its value irrespective of which term it is, is given by

$$\begin{aligned} & \text{Tr} \left\{ \prod_{k=1}^n [(R_{k1} + R_{k2})I - (R_{k3} + R_{k4})M_k] \right\} \\ & \times \text{Tr} \left\{ \prod_{k=1}^n [(R_{k1} - R_{k4})I + (R_{k2} - R_{k3})M_k] \right\} \\ & \times \prod_{k=1}^n (R_{k1} + R_{k2} - R_{k3} - R_{k4}), \end{aligned} \quad (4.8)$$

as the trace of a direct product is the product of the traces. The traces which appear in (4.8) are, for $n = 4$, of maximum degree 16 rather than 256 as in (4.7). The factor at the end is there because $X^3 = X$ for $X = \pm 1, 0$.

Now we know from group theory¹⁰ that these representations are reducible. These representations are made up of those whose Young tableaux contain at most two horizontal rows. In Table II we list the relevant irreducible representations, the number of times they occur, and their dimensionality for maximum cycle numbers of 2, 3, and 4. The necessary irreducible representations of the individual permutations required are tabulated in Hamermesh's book,¹⁰ or are easily derivable from those he does tabulate. It will be noted that the largest matrix we now need to consider is only 3×3 . We have programmed this procedure for the

computer, and it has produced in a systematic fashion the table of coefficients for each diagram from the string of loop permutations. We believe that this procedure is a reliable method of accomplishing what would be a very tedious and error-prone task by hand.

5. R -MATRIX PERTURBATION SERIES

The R -matrix series in terms of diagrams is simply derived. The first step is to write down all the diagrams in the potential series perturbation series. This job has been done through fourth order.⁷ Next we start in first order and group all the higher-order diagrams which correspond to the ladder insertions, with the first-order diagram.

TABLE II. The necessary irreducible representations.

	Irreducible representation	Number of occurrences	Dimension
$c = 2$	$\square\square$	3	1
	\square	1	1
	\square		
$c = 3$	$\square\square\square$	4	1
	$\square\square$	2	2
	\square		
$c = 4$	$\square\square\square\square$	5	1
	$\square\square\square$	3	3
	\square		
	$\square\square$	1	2
	$\square\square$		

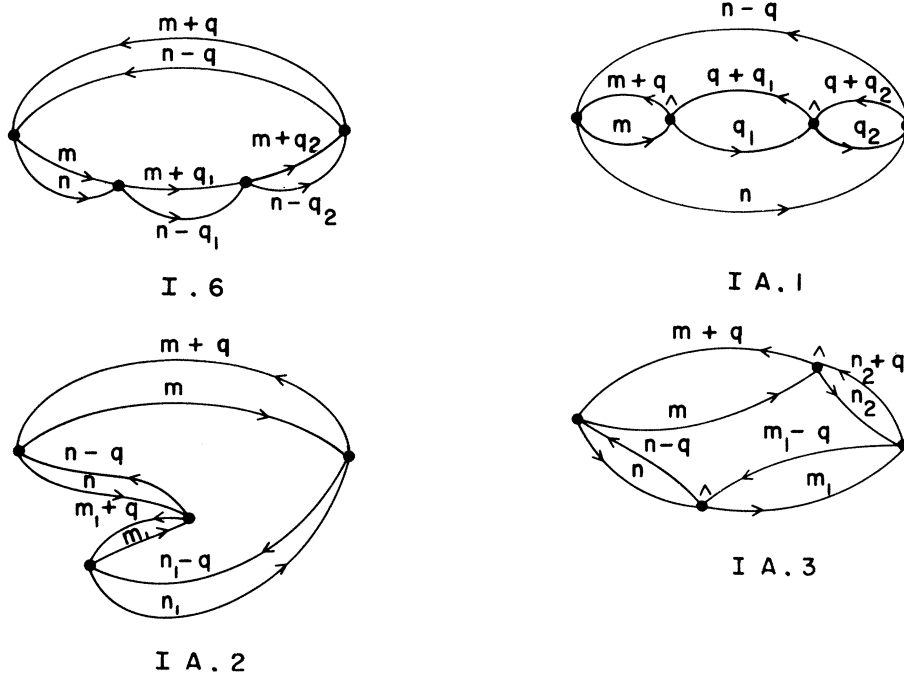


FIG. 7. R -matrix diagrams for classes I and IA of fourth order in the expansion.

This group will be the first-order K -matrix term. Then we proceed to the next order (third) and examine those diagrams which were not already grouped. To each of these we add those higher-order diagrams which correspond to ladder insertions in it. This procedure gives us a systematic procedure for developing the K -matrix series. Care must be exercised to sum all the different vertex orders together in situations like Fig. 4. Care must also be exercised to sum together all the diagrams with the same self-energy insertion in all the different filled-state and hole lines along a particular verti-

cal line, in order to avoid divergent terms. After this procedure has been carried out, we may expand the contribution of each K -matrix term in powers of R as explained in Sec. 2.

When this is done, the resultant diagrams have the topology of those of Ref. 7 numbered B1, R3, H3, F3, I.6, IA.1, IA.2, IA.3, II.3, II.4, II.5, II.7, II.8, II.9, II.10, II.11, II.12, IIA.1, IIA.2, IIA.3, IIA.4, IIA.5, IIA.6, III.2, III.9+10, IV.1, IV.4, IV.5, IV.6, and IV.7. The general term is, apart from a few diagrams with the opposite sign and a few cases in which it is convenient to group several Hugenholtz diagrams together,

$$\frac{-3(-1)^{P+H-C}}{16\pi(-4\pi)^n 2^m} \int d\vec{\tau} \frac{\text{Tr} \left[\prod_{k=1}^n (R_{k1} I \times I + R_{k2} I \times M_k - R_{k3} M_k \times M_k - R_{k4} M_k \times I) \right]}{\prod_{i=1}^{n-1} D_i}, \quad (5.1)$$

where the numerator is explained in the previous section, the denominator is the product of the various excitation energies, n is the order, m is the number of equivalent lines in the diagram, P is the number of violations of the Pauli principle, H is the number of holes, and C is the number of cycles.

We have illustrated the various diagrams in Figs. 6-10. The momenta are labeled and we have indicated which vertices require the inclusion of an excited Fermi sea in their evaluation by means of a carat over them in the figure. The value of the

sign factor in (5.1) of $(-1)^{P+H-C}$ is listed as a minus sign in front of the diagram name, where appropriate. The flag symbol always means that an \hat{R} matrix is required for the self-energy insertion on every filled-state line, but an R matrix is required on every hole line. Where we need to use the vertices in an order other than left to right for the reduction procedures of Sec. 4 to be valid, we have written the vertex order directly above the figure.

In the numerical approximations set out in Secs.

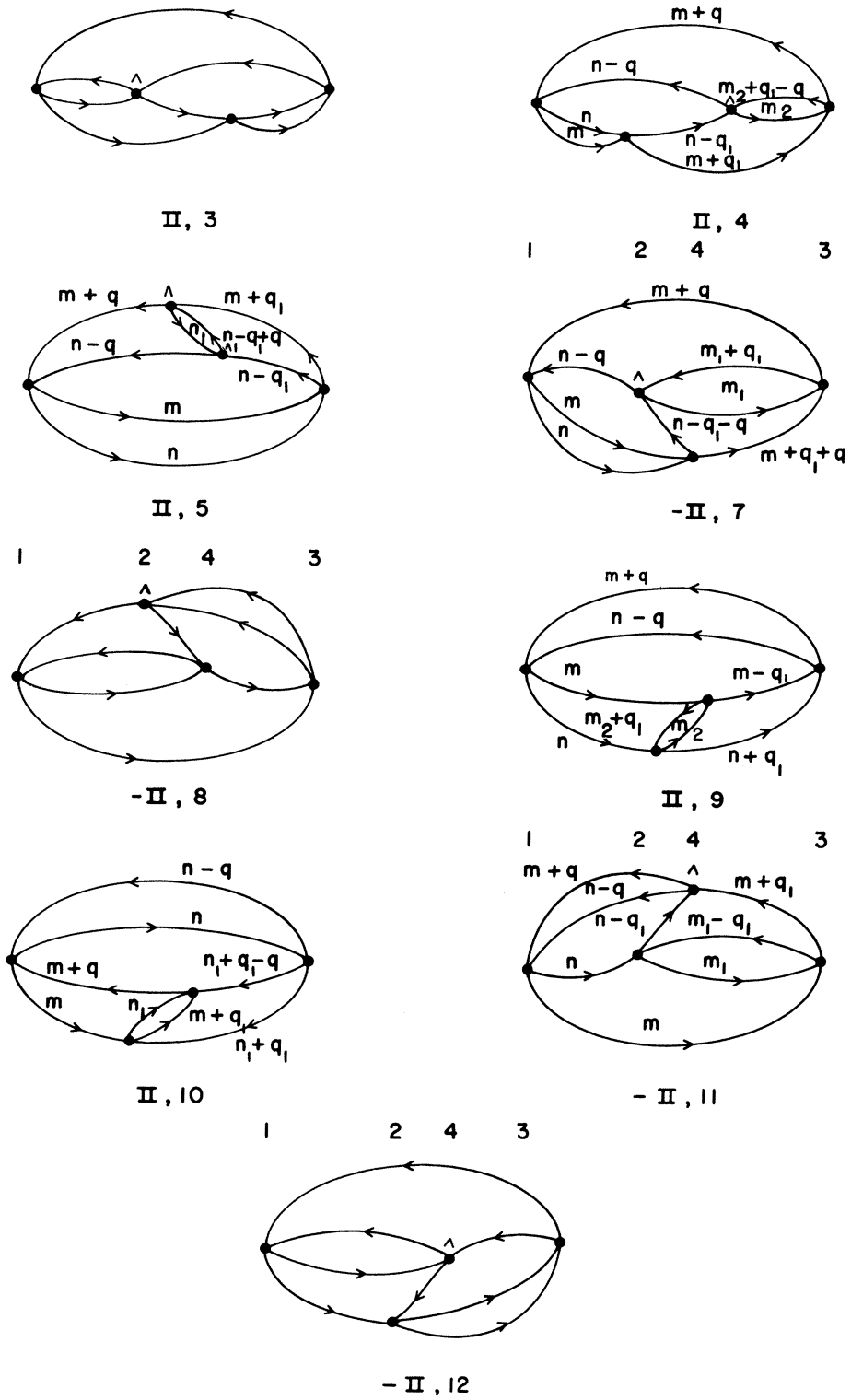


FIG. 8. R -matrix diagrams for class II of fourth order in the expansion. The superscript numbers are the straightened vertex order.

FIG. 9. R -matrix diagrams for class IIA of fourth order in the expansion. The superscript numbers are the straightened vertex order.

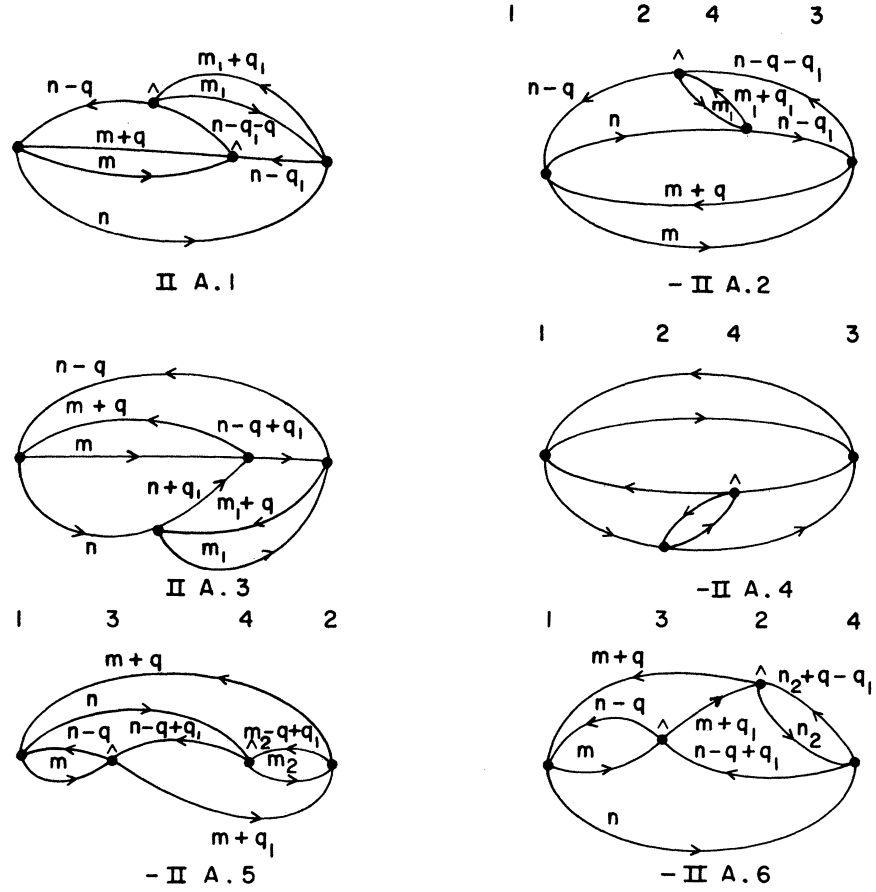


TABLE III. Momentum transfer table for the integrals.

Diagram	Permutations	c	$2k_2$	$2k'_2$	$2k_3$	$2k'_3$	$2k_4$	$2k'_4$
H3	(12) (12)	2	$2\vec{q}_1 + \vec{m} - \vec{n}$	$\vec{m} - \vec{n}$	$2\vec{q}_1 + \vec{m} - \vec{n}$	$2\vec{q} + \vec{m} - \vec{n}$		
R3	(23) (13)	3	$\vec{n} - \vec{q} - \vec{q}_1$	$\vec{n} + \vec{q} - \vec{q}_1$	$\vec{m} - \vec{q}_1$	$\vec{m} + 2\vec{q} - \vec{q}_1$		
I.6	(12) (12) (12)	2	$2\vec{q}_1 + \vec{m} - \vec{n}$	$\vec{m} - \vec{n}$	$2\vec{q}_2 + \vec{m} - \vec{n}$	$2\vec{q}_1 + \vec{m} - \vec{n}$	$2\vec{q}_2 + \vec{m} - \vec{n}$	$2\vec{q} + \vec{m} - \vec{n}$
IA.1	(13) (34) (24)	4	$\vec{m} + \vec{q} - \vec{q}_1$	$\vec{m} - \vec{q} - \vec{q}_1$	$\vec{q}_2 - \vec{q}_1 - \vec{q}$	$\vec{q}_2 + \vec{q} - \vec{q}_1$	$\vec{q}_2 - \vec{n}$	$2\vec{q} + \vec{q}_2 - \vec{n}$
IA.2	(34) (24) (13)	4	$\vec{m}_1 - \vec{n}_1$	$\vec{m}_1 + 2\vec{q} - \vec{n}_1$	$\vec{m}_1 - \vec{n}$	$2\vec{q} + \vec{m}_1 - \vec{n}$	$\vec{m} - \vec{n}_1$	$\vec{m} + 2\vec{q} - \vec{n}_1$
IA.3	(23) (14) (34)	4	$\vec{m}_1 - \vec{n} + \vec{q}$	$\vec{m}_1 - \vec{q} - \vec{n}$	$\vec{m} + \vec{q} - \vec{n}_2$	$\vec{m} - \vec{n}_2 - \vec{q}$	$\vec{m}_1 - \vec{n}_2$	$\vec{m}_1 - 2\vec{q} - \vec{n}_2$
II.4	(12) (23) (13)	3	$2\vec{q}_1 + \vec{m} - \vec{n}$	$\vec{m} - \vec{n}$	$\vec{m}_2 - \vec{n} + \vec{q}$	$\vec{m}_2 + 2\vec{q}_1 - \vec{q} - \vec{n}$	$\vec{m} + \vec{q}_1 - \vec{m}_2$	$\vec{m} + 2\vec{q} - \vec{m}_2 - \vec{q}_1$
II.5	(13) (23) (12)	3	$\vec{m} + \vec{q} - \vec{n}_1$	$\vec{m} + 2\vec{q}_1 - \vec{n}_1 - \vec{q}$	$\vec{n}_1 - \vec{n} + \vec{q}_1$	$2\vec{q} + \vec{n}_1 - \vec{q}_1 - \vec{n}$	$\vec{m} - \vec{n}$	$2\vec{q}_1 + \vec{m} - \vec{n}$
II.7	(23) (13) (12)	3	$\vec{m}_1 - \vec{n} + \vec{q}$	$2\vec{q}_1 + \vec{q} + \vec{m}_1 - \vec{n}$	$\vec{m} + \vec{q}_1 + \vec{q} - \vec{m}_1$	$\vec{m} + \vec{q} - \vec{m}_1 - \vec{q}_1$	$\vec{m} - \vec{n}$	$\vec{m} + 2\vec{q}_1 + 2\vec{q} - \vec{n}$
II.9	(23) (13) (12)	3	$\vec{m}_2 - \vec{n} - \vec{q}_1$	$\vec{m}_2 + \vec{q}_1 - \vec{n}$	$\vec{m} - \vec{m}_2$	$\vec{m} - \vec{m}_2 - 2\vec{q}_1$	$\vec{m} - 2\vec{q}_1 - \vec{n}$	$\vec{m} + 2\vec{q} - \vec{n}$
II.10	(13) (13) (23)	3	$\vec{m} + \vec{q}_1 - \vec{n}_1$	$\vec{m} - \vec{n}_1 - \vec{q}_1$	$\vec{m} + \vec{q}_1 - \vec{n}_1$	$\vec{m} + 2\vec{q} - \vec{n}_1 - \vec{q}_1$	$\vec{n} - \vec{n}_1 - \vec{q}_1 + \vec{q}$	$\vec{n} - \vec{q} - \vec{n}_1 - \vec{q}_1$
II.11	(23) (13) (12)	3	$\vec{m}_1 - \vec{n} + \vec{q}_1$	$\vec{m}_1 - \vec{q}_1 - \vec{n}$	$\vec{m} - \vec{m}_1$	$\vec{m} + 2\vec{q}_1 - \vec{m}_1$	$\vec{m} + 2\vec{q}_1 - \vec{n}$	$\vec{m} + 2\vec{q} - \vec{n}$
IIA.1	(23) (12) (23)	3	$\vec{m}_1 - \vec{n} + \vec{q}$	$\vec{m}_1 + 2\vec{q}_1 - \vec{n} + \vec{q}$	$\vec{m} - \vec{n} + \vec{q}_1$	$\vec{m} + 2\vec{q} - \vec{n} + \vec{q}_1$	$\vec{m}_1 - \vec{n}$	$\vec{m}_1 + 2\vec{q}_1 - \vec{n}$
IIA.2	(23) (12) (23)	3	$\vec{m}_1 - \vec{n} + \vec{q}$	$\vec{m}_1 + 2\vec{q}_1 + \vec{q} - \vec{n}$	$\vec{m} + \vec{q}_1 - \vec{n}$	$\vec{m} + 2\vec{q} + \vec{q}_1 - \vec{n}$	$\vec{m}_1 - \vec{n}$	$\vec{m}_1 + 2\vec{q}_1 - \vec{n}$
IIA.3	(23) (12) (23)	3	$\vec{m}_1 - \vec{n} - \vec{q}_1$	$\vec{m}_1 + \vec{q}_1 - \vec{n}$	$\vec{m} - \vec{n} - \vec{q}_1$	$\vec{m} + 2\vec{q} - \vec{n} - \vec{q}_1$	$\vec{m}_1 - \vec{n} + \vec{q} - \vec{q}_1$	$\vec{m}_1 + \vec{q}_1 - \vec{n} + \vec{q}$
IIA.5	(13) (12) (13)	3	$\vec{m} + \vec{q}_1 - \vec{m}_2$	$\vec{m} + 2\vec{q} - \vec{m}_2 - \vec{q}_1$	$\vec{n} - \vec{q} - \vec{m} - \vec{q}_1$	$\vec{n} - \vec{m} + \vec{q}_1 - \vec{q}$	$\vec{m}_2 - \vec{n} + \vec{q} - \vec{q}_1$	$\vec{m}_2 - \vec{q} + \vec{q}_1 - \vec{n}$
IIA.6	(13) (12) (13)	3	$\vec{m} + \vec{q} - \vec{n}_2$	$\vec{m} + 2\vec{q}_1 - \vec{n}_2 - \vec{q}$	$\vec{m} + \vec{q}_1 - \vec{n} + \vec{q}$	$\vec{m} - \vec{n} + \vec{q} - \vec{q}_1$	$\vec{n}_2 - \vec{n}$	$\vec{n}_2 + 2\vec{q} - 2\vec{q}_1 - \vec{n}$
III.2	(23) (23) (12)	3	$\vec{m}_1 - \vec{n}_1$	$\vec{m}_1 + \vec{n}_1 - 2\vec{n}$	$\vec{m}_1 - \vec{n}_1$	$\vec{m}_1 + \vec{n}_1 - 2\vec{n}$	$\vec{m} - \vec{n}$	$\vec{m} + 2\vec{q} - \vec{n}$
III.9 + 10	(13) (13) (12)	3	$\vec{m}_1 - \vec{n}_1$	$2\vec{m} + 2\vec{q} - \vec{m}_1 - \vec{n}_1$	$\vec{m}_1 - \vec{n}_1$	$2\vec{m} + 2\vec{q} - \vec{m}_1 - \vec{n}_1$	$\vec{m} - \vec{n}$	$\vec{m} + 2\vec{q} - \vec{n}$

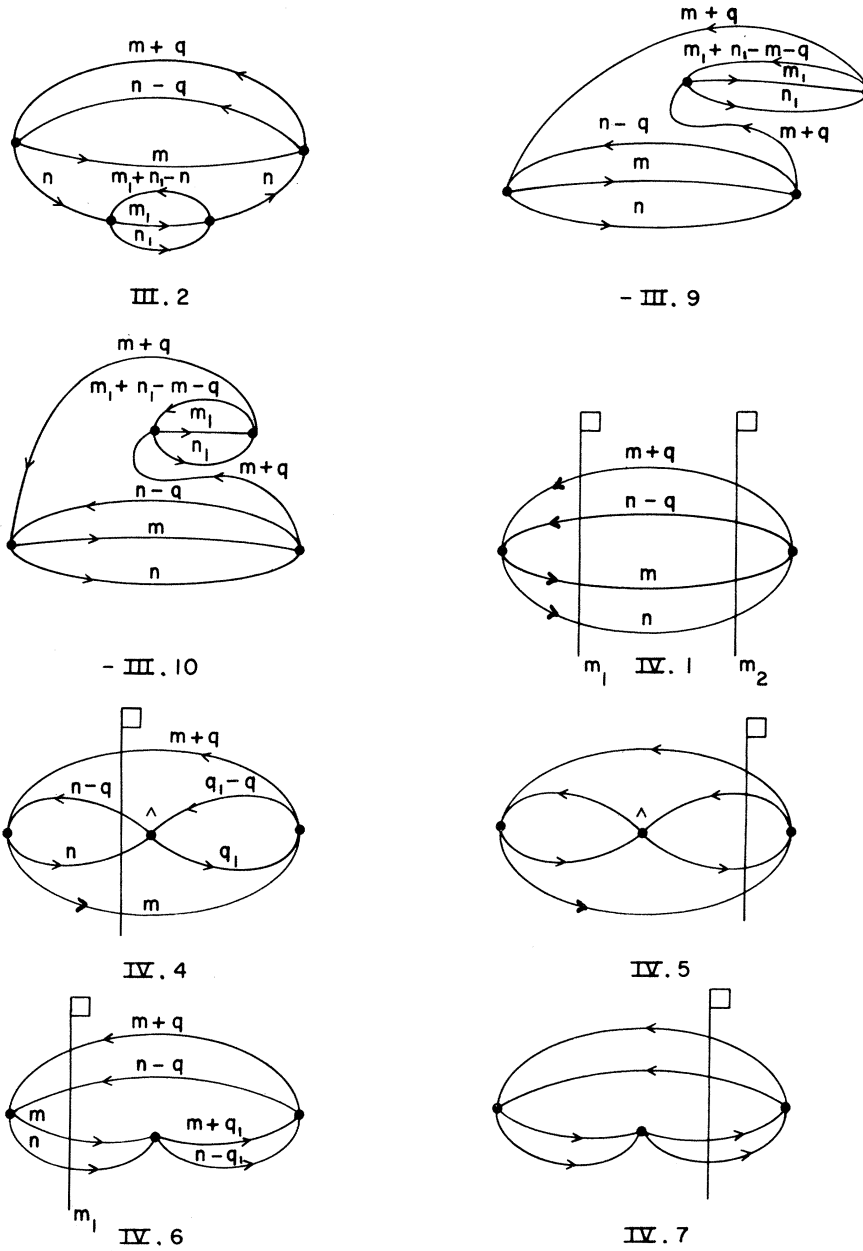


FIG. 10. R -matrix diagrams for classes III and IV of fourth order in the expansion.

2 and 3 each R_{kj} depends on the initial relative momentum, \vec{k} , and the final relative momentum vector \vec{k}' . We have tabulated these in Table III. These are derived in the main from the paper of Baker, Hill, and McKee,¹¹ where the momentum transfer and the exchanged momentum transfer are tabulated; however, the relative signs listed there are not always consistent, as their functions do not depend on this sign. For all diagrams we have

$$\vec{k}_1 = \frac{1}{2}(\vec{m} - \vec{n}), \quad \vec{k}'_1 = \frac{1}{2}(\vec{m} + \vec{q} - \vec{n}). \tag{5.2}$$

The M_k matrices are described by the permutations in Table III. The permutation at the first vertex is always (12), and so is omitted.

All the required denominators D_i in (5.1) are tabulated in Ref. 7, to which the reader is referred. The notation has been kept the same. The region

of integration in (5.1) is defined by the Pauli principle, which states

$$|\vec{m}| \leq k_F, \quad |\vec{v}| > k_F, \quad (5.3)$$

where \vec{m} is any hole momentum (line with an arrow to the right) and \vec{v} is any filled-state momentum (line with an arrow to the left in Figs. 6-10). The vertex order in Table III is the straightened order, where that order differs from the left to right order.

We will now discuss the diagrams listed at the beginning of this section which do not appear in Table III. Diagram B1 has been thoroughly discussed in Sec. 2. The contribution from the following diagrams is identical to that of another, but must be included to obtain the correct total. Hence we only calculate one of each pair, II.3=II.4, II.7=II.12, II.8=II.11, IIA.2=IIA.4, IV.4=IV.5, IV.6=IV.7. The remaining diagrams not yet discussed represent the sum of several Hugenholtz diagrams each, and consequently the form (5.1) is modified appropriately. All of these diagrams are the sum of the same self-energy bubble acting on all lines in a given vertex position. The factor for this vertex is obtained by replacing R_{k_j} ($j=1-4$) by the sum of the appropriate \hat{R} 's for the filled-state lines *minus* the sum of the appropriate R 's for the hole lines.

Thus for F3 we get

$$\begin{aligned} \vec{k}_1 = \vec{k}_3 = \frac{1}{2}(\vec{m} - \vec{n}), \quad \vec{k}'_1 = \vec{k}'_3 = \frac{1}{2}(\vec{m} + 2\vec{q} - \vec{n}), \\ \vec{k}_{2A} = \vec{k}'_{2A} = \frac{1}{2}(\vec{q}_1 - \vec{m} - \vec{q}), \quad \vec{k}_{2B} = \vec{k}'_{2B} = \frac{1}{2}(\vec{q}_1 - \vec{m}). \end{aligned} \quad (5.4)$$

The subscript 2A refers to the filled state $+\hat{R}$ contribution at vertex 2, and the subscript 2B refers to the $-R$ contribution at vertex 2. In addition, we have an extra factor of 2, as the bubble could have been on either of the two equivalent filled-state (or hole) lines. The minus sign that comes in front of the bubble on the hole line arises from the Pauli principle.

For diagram IV.1 we have

$$\begin{aligned} \vec{k}_1 = \vec{k}_4 = \frac{1}{2}(\vec{m} - \vec{n}), \quad \vec{k}'_1 = \vec{k}'_4 = \frac{1}{2}(\vec{m} + 2\vec{q} - \vec{n}), \\ \vec{k}_{2A} = \vec{k}'_{2A} = \frac{1}{2}(\vec{m} + \vec{q} - \vec{m}_1), \quad \vec{k}_{2B} = \vec{k}'_{2B} = \frac{1}{2}(\vec{n} - \vec{q} - \vec{m}_1), \\ \vec{k}_{2C} = \vec{k}'_{2C} = \frac{1}{2}(\vec{m} - \vec{m}_1), \quad \vec{k}_{2D} = \vec{k}'_{2D} = \frac{1}{2}(\vec{n} - \vec{m}_1), \quad (5.5) \\ \vec{k}_{3A} = \vec{k}'_{3A} = \frac{1}{2}(\vec{m} + \vec{q} - \vec{m}_2), \quad \vec{k}_{3B} = \vec{k}'_{3B} = \frac{1}{2}(\vec{n} - \vec{q} - \vec{m}_2), \\ \vec{k}_{3C} = \vec{k}'_{3C} = \frac{1}{2}(\vec{m} - \vec{m}_2), \quad \vec{k}_{3D} = \vec{k}'_{3D} = \frac{1}{2}(\vec{n} - \vec{m}_2). \end{aligned}$$

In this diagram the subscripts *A* and *B* refer to filled states, and *C* and *D* refer to holes.

For diagram IV.4 we have \vec{k}_1 and \vec{k}'_1 given by (5.2) and \vec{k}_{2A} , \vec{k}'_{2A} , \vec{k}_{2B} , \vec{k}'_{2B} , \vec{k}_{2C} , \vec{k}'_{2C} , \vec{k}_{2D} , and \vec{k}'_{2D} given by (5.5). The rest are

$$\begin{aligned} \vec{k}_3 = \frac{1}{2}(\vec{n} - \vec{q} - \vec{q}_1), \quad \vec{k}'_3 = \frac{1}{2}(\vec{q}_1 - \vec{q} - \vec{n}), \\ \vec{k}_4 = \frac{1}{2}(\vec{m} - \vec{q}_1), \quad \vec{k}'_4 = \frac{1}{2}(\vec{m} + 2\vec{q} - \vec{q}_1). \end{aligned} \quad (5.6)$$

Again the *A* and *B* subscripts refer to filled states, and the *C* and *D* refer to holes.

For the last diagram, IV.6, k_1 and k'_1 are given by (5.2), and \vec{k}_{2A} , \vec{k}'_{2A} , \vec{k}_{2C} , and \vec{k}'_{2C} are given by (5.5). The rest are

$$\begin{aligned} \vec{k}_3 = \frac{1}{2}(\vec{m} + 2\vec{q}_1 - \vec{n}), \quad \vec{k}'_3 = \frac{1}{2}(\vec{m} - \vec{n}), \\ \vec{k}_4 = \frac{1}{2}(\vec{m} + 2\vec{q}_1 - \vec{n}), \quad \vec{k}'_4 = \frac{1}{2}(\vec{m} + 2\vec{q} - \vec{n}). \end{aligned} \quad (5.7)$$

Here *A* refers to a filled state and *C* to a hole. This diagram requires an additional factor of 2 for correct counting due to two pairs of equivalent lines. We have listed the permutations required to describe the M_k in Table IV. Again the permutation of the first vertex is always (12), and so is omitted.

If no approximations were used in the computation of \hat{R} , then it would reduce to R when all the lines meeting at that vertex lie in the surface of the Fermi sea. This property is important, as there is a related vanishing of the relevant D_i at the same time. If our approximation (the use of an averaged excitation energy) should destroy this property of \hat{R} (as it does), then we would introduce spurious singularities into the integrand of (5.1). To prevent this undesirable behavior, we have modified the definition of \hat{R} in diagrams F3, IV.1, IV.4, and IV.6 as follows

$$\begin{aligned} \langle \pm \vec{k} | \hat{R}_{\text{modified}} | \vec{k} \rangle &= \frac{D_1 \langle \pm \vec{k} | \hat{R} | \vec{k} \rangle + [k^2 + \Delta(k) - D_1] \langle \pm \vec{k} | R | \vec{k} \rangle}{k^2 + \Delta(k)}, \\ & \quad k \leq k_F, \\ & = \langle \pm k | R | k \rangle \quad k > k_F. \end{aligned} \quad (5.8)$$

The denominator D_1 happens to be (or is equal to)

TABLE IV. Permutations specifying M_k .

Diagram	Permutations	<i>c</i>
F3	(23) (12)	3
IV.1	(23) (24) (12)	4
IV.4	(14) (23) (13)	4
IV.6	(13) (12) (12)	3

the correct relevant vanishing denominator in the aforementioned diagrams, and this modification serves to make \hat{R} equal to R at the right points. It will be noted that by (4.6), (5.4), and (5.5) that only the matrix elements $\langle \pm \vec{k} | \hat{R}_{\text{modified}} | \vec{k} \rangle$ are required; the off-energy-shell elements do not enter into these diagrams.

The integration for each diagram was done by a Monte Carlo procedure. We select the independent momenta in the Fermi sea, \vec{m} for example, according to the prescription that $m^s = k_F^s r_1$, where r_1 is a random number which is distributed uniformly on the interval (0, 1). For momenta which can be infinite, we select a filled-state momentum, say $|\vec{m} + \vec{q}| = k_F r_2^{-E}$, where r_2 is again a random number which is uniformly distributed on the interval (0, 1). The set of momenta selected in this way are then tested to retain only those points which also satisfy the restrictions due to the Pauli principle and which are not automatically taken care of by our selection procedure. The cosine of the angles between independent momenta has been taken as uniformly distributed.

Only in two diagrams is special comment required on the integration procedures. In II.5 and IIA.1 (where "real" three-body scattering occurs) there are two independent momenta which become infinite instead of just unity as in the other diagrams. Here we select instead

$$\begin{aligned} |\vec{m} + \vec{q}| &= k_F Q \cos \Phi, & |\vec{m} + \vec{q}_1| &= k_F Q \sin \Phi, \\ Q &= \sqrt{2}/r_1^E, & \Phi &= \frac{1}{2}\pi r_2. \end{aligned} \quad (5.9)$$

This choice is necessary to make the integral doable by a Monte Carlo procedure. Because of the hard core the quantity \hat{R} which comes in does not vanish at infinity, and hence these special additional precautions are necessary to assure a convergent numerical procedure.

As a test to determine whether our programming of the diagrams was correct, we have also specialized *every diagram* to the case of spin only (no isospin); we use the spin-independent repulsive square-well force of Baker, Gammel, and Hill⁷ in place of the R and \hat{R} matrix elements. We can then compare our results directly with theirs and check whether we get the same answer. The specialization was accomplished by using the one-dimensional representation $P_{ij}(\epsilon) \equiv 1$ in (5.1). Also, by (4.6)

$$\begin{aligned} R_{j,1} &= v(q_j), & R_{j,3} &= v(q_{j, \text{exch}}), \\ R_{j,2} &= R_{j,4} = 0, \end{aligned} \quad (5.10)$$

where q_j is the momentum transfer and $q_{j, \text{exch}}$ is the exchanged momentum transfer at the j th vertex,

and $v(q)$ is the momentum transfer of the potential function.

At this point we would like to thank Crichton and Anderson¹² for pointing out that Eq. (2.15) of Ref. 7 for diagrams IIA.5-6 is wrong and that the form given there for diagrams IIA.1-4 is also correct for IIA.5-6. We cannot therefore use this test on IIA.5-6. We note that this particular error does not persist in Ref. 11.

The application of our test procedure has turned up two additional minor errors in previous work (Refs. 7 and 11), as well as eliminating a number of potential errors in this work. The entry for κ_2 for diagram II.9 in Table II of Ref. 7 should have been $|\vec{q} + \vec{q}_1|$ instead of $|\vec{q} - \vec{q}_1|$. Also one of the Pauli restrictions was wrongly programmed in diagram IIA.2 (= IIA.4). These errors also persist in Ref. 11. The numerical effect of all these errors on previous work is rather small.

The integrals were evaluated by using 10^5 to 10^6 Monte Carlo values of each integrand.

6. NUMERICAL VALUES

In this section we tabulate the numerical values of the coefficients of the R -matrix expansion described in the previous sections for the potential described by (2.1)-(2.3). We also analyze these coefficients and discuss their implication for the ground-state energy function.

We have only computed the higher-order terms of R -matrix expansion for the first-order K -matrix diagram. As the leading corrections here are very small, we have not calculated the first-order corrections to the third-order diagrams, which should be done to complete the expansion through fourth order. Other than that, we have a complete expansion through fourth order. In Table V we have listed our best values for the integrals through third order for various densities. In Table VI we give our best values for the fourth-order integrals at a density of $k_F c = 0.625$, which, we believe, is close to saturation for this potential. The errors quoted are one standard deviation observed in the Monte Carlo evaluations.

In order to analyze what these data imply about the ground-state energy of a many-fermion system interacting with this potential, we need to sum the R -matrix series. To do this, we shall use the Padé approximant method.¹³ An assessment of the accuracy to be expected has been obtained by means of a model calculation² on a lattice gas. There it was found that, while the lowest-order approximations were rather wide of the mark, improvement was quite rapid, and by the time fourth-order terms were taken into account in the region of interest here, the saturation density was locat-

TABLE V. R -matrix expansion data (units 1=259.2 MeV).

Diagram	$k_{FC}=0.5$		$k_{FC}=0.625$		$k_{FC}=0.75$		$k_{FC}=0.875$	
	Value	Deviation	Value	Deviation	Value	Deviation	Value	Deviation
Zero order ($0.3k_F^2c^2$) ^a	0.075		0.117 19		0.168 75		0.229 69	
First order B1 ^a	-0.1560		-0.2492		-0.3537		-0.4366	
Second order B1 ^a	1.1379×10^{-3}		5.098×10^{-4}		-1.507×10^{-5}		1.194×10^{-3}	
Third order B1 ^a	-1.666×10^{-4}		-1.102×10^{-4}		-1.084×10^{-4}		-1.602×10^{-4}	
H3	-3.370×10^{-3}	$\pm 6 \times 10^{-5}$	-4.472×10^{-3}	$\pm 9 \times 10^{-5}$	-7.92×10^{-3}	$\pm 1.3 \times 10^{-4}$	-1.191×10^{-2}	$\pm 2.5 \times 10^{-4}$
R3	-1.22×10^{-3}	$\pm 6 \times 10^{-5}$	6.09×10^{-4}	$\pm 1.7 \times 10^{-4}$	1.53×10^{-2}	$\pm 6 \times 10^{-4}$	7.88×10^{-2}	$\pm 1.7 \times 10^{-3}$
F3 ^{a,b}	5.33×10^{-2}	$\pm 3.6 \times 10^{-4}$	1.29×10^{-1}	$\pm 1.3 \times 10^{-3}$	3.26×10^{-1}	$\pm 2.6 \times 10^{-3}$	7.44×10^{-1}	$\pm 7.7 \times 10^{-3}$
Total	4.85×10^{-2}	$\pm 3.7 \times 10^{-4}$	1.25×10^{-1}	$\pm 1.3 \times 10^{-3}$	3.33×10^{-1}	$\pm 2.6 \times 10^{-3}$	8.11×10^{-1}	$\pm 7.9 \times 10^{-3}$

^aTerms included in the Brueckner approximation.

^bExcept for this term, which is only partly included, the other terms listed in this table as included in the Brueckner approximation are also included in the two-“hole-line” approximation of the Cornell group.

ed to an accuracy of about 2%. The energy is obtained with relatively greater accuracy.

We have shown in Fig. 11 a plot of our results for successively more accurate Padé approximants. The most accurate Padé approximants are

$$\begin{aligned} [2, 2] &= -25.6 \text{ MeV}, \\ [1, 3] &= -24.3 \text{ MeV}, \end{aligned} \quad (6.1)$$

for $k_{FC} = 0.625$.

By way of a check we have also used the Borel method of summing divergent series.¹⁴ Analytic continuation at an intermediate stage was provided by a $[2, 2]$ Padé approximant. The result was -25.7 MeV. These results are to be compared with those obtained by the “hole-line” approximation^{15, 16} using the Brandow choice¹⁷ for intermediate-state energies. For this potential⁶ it is, in two-“hole-line” approximation, -16.76 MeV at $k_{FC} = 0.625$. We have discussed in Ref. 6 the reasons why we do not feel that one may confidently use the “hole-line” approximation to evaluate the many-body energy. The source of the difficulty appears to lie in the treatment of the energy in the intermediate states. Inspection of Tables V and VI reveals that, at least in low order, the “hole-line” selection criteria works well in selecting the largest diagrams. By this we mean that those diagrams either wholly or partially included in the two- and three-“hole-line” approximations are indeed the largest diagrams. (All third-order diagrams are included in the three-hole-line approximation.) It is not possible with our results to give an order-by-order assessment of the terms neglected in the

“hole-line” approximations with the Brandow choice¹⁷ for the intermediate-state energies because only parts of certain diagrams are included.

We have previously discussed⁷ the difficulty with the approach of Brueckner and Gammel.¹⁸ In addition, Bethe¹⁹ has emphasized the importance of including the three-body scattering terms, such as IIA.1 of Table VI which is around 40 MeV in size.

In conclusion, we showed in a previous paper⁶ that the R -matrix expansion^{1, 2} defines the physically correct energy, at least for densities and inter-

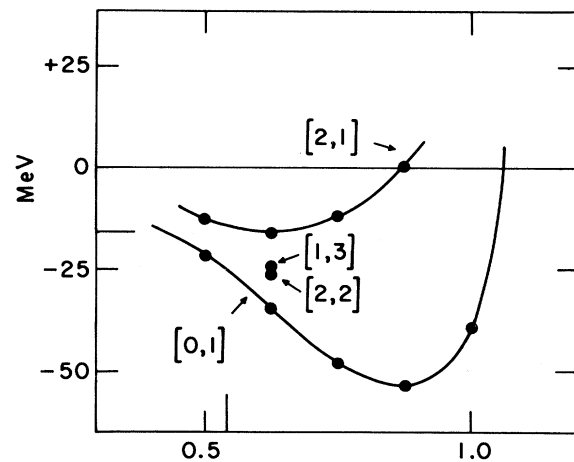


FIG. 11. Padé approximants to the binding energy of the many-fermion system using our model force. The large tick marks are the experimental “nuclear matter” density and energy.

TABLE VI. Fourth-order R -matrix expansion data for $k_{FC} = 0.625$ (units $1 = 259.2$ MeV).

Diagram	Value	Deviation
B1	5.084×10^{-6}	
I.6	-2.66×10^{-4}	$\pm 8 \times 10^{-6}$
IA.1	-2.52×10^{-3}	$\pm 9.5 \times 10^{-5}$
IA.2	-1.56×10^{-3}	$\pm 5.5 \times 10^{-5}$
IA.3	-2.37×10^{-3}	$\pm 1.2 \times 10^{-4}$
II.3	6.1×10^{-5}	$\pm 9 \times 10^{-6}$
II.4 ^a	6.1×10^{-5}	$\pm 9 \times 10^{-6}$
II.5 ^b	-9.1×10^{-3}	$\pm 5 \times 10^{-4}$
II.7 ^b	-1.40×10^{-4}	$\pm 7 \times 10^{-6}$
II.8	-2.29×10^{-4}	$\pm 2.8 \times 10^{-5}$
II.9	-7.7×10^{-5}	$\pm 6 \times 10^{-6}$
II.10	2.0×10^{-5}	$\pm 5 \times 10^{-6}$
II.11 ^a	-2.29×10^{-4}	$\pm 2.8 \times 10^{-5}$
II.12 ^{a,b}	-1.40×10^{-4}	$\pm 7 \times 10^{-6}$
IIA.1 ^b	-0.1516	$\pm 9.5 \times 10^{-4}$
IIA.2	-5.3×10^{-4}	$\pm 4 \times 10^{-5}$
IIA.3	-6.4×10^{-4}	$\pm 5 \times 10^{-5}$
IIA.4 ^a	-5.3×10^{-4}	$\pm 4 \times 10^{-5}$
IIA.5	4.45×10^{-3}	$\pm 8.5 \times 10^{-5}$
IIA.6	4.32×10^{-3}	$\pm 1.0 \times 10^{-4}$
III.2	-3.23×10^{-3}	$\pm 9 \times 10^{-5}$
III.9 + 10	3.68×10^{-3}	$\pm 7.5 \times 10^{-5}$
IV.1 ^{c,d,e}	-0.1117	$\pm 8.5 \times 10^{-4}$
IV.4	8.6×10^{-3}	$\pm 2.5 \times 10^{-4}$
IV.5 ^{a,e}	8.6×10^{-3}	$\pm 2.5 \times 10^{-4}$
IV.6 ^e	-1.637×10^{-2}	$\pm 3.5 \times 10^{-4}$
II.7 ^{a,e}	-1.637×10^{-2}	$\pm 3.5 \times 10^{-4}$
Total	-0.2878	$\pm 1.6 \times 10^{-3}$

^aIdentical to a previous diagram (but must be added to find the total fourth-order coefficient).

^bIncluded in the three-“hole-line” approximation.

^cIncluded in the Brueckner approximation.

^dPartially included in the two-“hole-line” approximation.

^ePartially included in the three-“hole-line” approximation.

action strengths where the many-fermion system is free of long-range order (diagonal or off-diagonal). By “defines” we mean that there is at most one function of a suitably restricted class which has that expansion. We have calculated the first four terms of this expansion for a model hard-core potential and obtain a binding energy of about -25 MeV with an uncertainty of perhaps several MeV. This energy is significantly more attractive than that given by the two-“hole-line” approximation for the same potential. Previously¹⁶ that approximation was found, for good hard-core potentials, to yield too little binding energy for the nuclear-matter problem. Soft-core potentials have been found^{11,16} to be more attractive, and to yield²⁰ in that approximation results for the nuclear-matter problem which are closer to experimental values. In light of our present results, it seems that it is rather likely that the correct many-fermion binding energy is significantly more attractive than the “hole-line” approximation, with the Brandow choice for the intermediate-state energies, indicates and that the hard-core potentials are not incompatible with the observed binding energy for the nuclear-matter problem.

ACKNOWLEDGMENTS

The authors wish to acknowledge helpful conversations with J. L. Gammel, H. A. Bethe, and A. Kerman.

*This work was performed under the auspices of the U. S. Atomic Energy Commission.

¹G. A. Baker, Jr., Phys. Rev. **140**, B9 (1965).

²G. A. Baker, Jr., and J. Kahane, J. Math. Phys. **10**, 1647 (1969).

³K. A. Brueckner, in *The Many Body Problem*, edited by C. Dewitt (John Wiley & Sons, Inc., New York, 1959).

⁴K. A. Brueckner and K. S. Masterson, Jr., Phys. Rev. **128**, 2267 (1962).

⁵G. A. Baker, Jr., Phys. Rev. **131**, 1869 (1963).

⁶G. A. Baker, Jr., J. Math. Phys. **11**, No. 7 (1970).

⁷G. A. Baker, Jr., J. L. Gammel, and B. J. Hill, Phys. Rev. **132**, 1373 (1963).

⁸P. M. Morse and H. Feshbach, *Methods of Theoretical Physics* (McGraw-Hill Book Company, Inc., New York, 1953), Part II.

⁹N. M. Hugenholtz, Physica **23**, 481 (1957).

¹⁰M. Hamermesh, *Group Theory and its Application to Physical Problems* (Addison-Wesley Publishing Company, Reading, Massachusetts, 1962).

¹¹G. A. Baker, Jr., B. J. Hill, and R. J. McKee, Jr., Phys. Rev. **135**, A922 (1964).

¹²J. H. Crichton and R. H. Anderson, private communication, 1967.

¹³For a general review, including early applications to the many-fermion problem, see G. A. Baker, Jr., Advan. Theoret. Phys. **1**, 1 (1965); and more recently, *The Padé Approximant in Theoretical Physics*, edited by G. A. Baker, Jr., and J. L. Gammel (Academic Press Inc., New York, to be published).

¹⁴G. H. Hardy, *Divergent Series* (Oxford University Press, London, England, 1956).

¹⁵B. D. Day, Rev. Mod. Phys. **39**, 719 (1967).

¹⁶R. Rajaraman and H. A. Bethe, Rev. Mod. Phys. **39**, 745 (1967).

¹⁷B. H. Brandow, Phys. Rev. **152**, 863 (1966).

¹⁸K. A. Brueckner and J. L. Gammel, Phys. Rev. **109**, 1040 (1958).

¹⁹H. A. Bethe, Phys. Rev. **138**, B804 (1965).

²⁰H. A. Bethe, private communication, 1969.